Life Sciences 234 (2019) 116756

Contents lists available at ScienceDirect

Life Sciences

journal homepage: www.elsevier.com/locate/lifescie

Silica-coated iron oxide nanoparticles as a novel nano-radiosensitizer for electron therapy

Mohamed M. Fathy[a], Heba M. Fahmy[a,*], Omnia A. Saad[a], Wael M. Elshemey[a,b]

[a] Biophysics Department, Faculty of Science, Cairo University, 12613 Giza, Egypt
[b] Department of Physics, Faculty of Science, Islamic University in Madinah, kSA

ARTICLE INFO

Keywords:
Iron oxide magnetic nanoparticles (IO-MNPs)
Silica-coated iron oxide magnetic nanoparticles (SIO-MNPs)
Radiation therapy
Nano-radiosensitizer
Breast cancer
MTT assay
Comet assay

ABSTRACT

Aims: Conventional radiotherapy is mainly restricted by the low radiation absorption efficiency of tumors tissues and the hypoxic tumor cells radio-resistance. In this paper, novel nano-radiosensitizers, magnetic nanoparticles core coated with silica, were successfully prepared to overcome these limitations.
Main methods: The prepared nanoparticles have been characterized by transmission electron microscope (TEM), Dynamic light scattering (DLS), atomic force microscope (AFM) and vibration sample magnetometer (VSM). MTT cytotoxicity and DNA double-strand breaks (Comet) assays have been used to assess the radio-enhancing effect of iron oxide magnetic nanoparticles (IO-MNPs) and silica-coated iron oxide magnetic nanoparticles (SIO-MNPs) against MCF7 breast cancer cells. MCF7 cells were treated with different concentrations of the prepared nanoformulations and exposed to an electron beam at doses 0, 0.5, 1, 2, 4 Gy.
Key findings: DLS measurements revealed that the main hydrodynamic diameter of the prepared IO-MNPs and SIO-MNPs was 18.17 ± 4.5 nm and 164.18 ± 16.1 nm, respectively, which was confirmed by TEM micrographs. MTT and comet assays results showed that the radiosensitizing effect of the prepared nanoformulations was dose and concentration dependent. Interestingly, the dose enhancement factor (DEF) for SIO-MNPs was, on average, 1.3-fold greater than that of IO-MNPs.
Significance: Coating of IO-MNPs with silica led to enhance their electron radiosensitization and consequently their therapeutic efficacy. Therefore, SIO-MNPs represent a promising engineered nano-formulation for enhancing breast cancer radiosensitivity.

1. Introduction

Cancer is one of the most remarkable causes of death globally, Breast cancer is the most widespread malignancy which is the major reason for cancer-related deaths in females worldwide [1–3]. For more than a century, one of the most widely used, non-surgical procedures in cancer therapy was the radiation therapy [4].

The primary aim of radiation therapy (RT) is the reduction of delivering dose for surrounding healthy tissues [5,6].

Because of the intrinsic radioresistance of cancer cells, radiation dose needs to be increased, but this can lead to early and long-term side-effects restricting its medical utilization and so, RT is not effective against cancers like breast cancer and glioblastoma [7,8]. This is considered as an obstacle, which embed the use of RT alone to treat tumors [9,10].

Recently, there have been several attempts to enhance the clinical outcome of radiotherapy using the high-atomic number nanoparticles as radiosensitizer agents in cells [11] due to their ability to increase the efficiency of radiation therapy of cancerous cells through enhancing the production of reactive oxygen species (ROS) [12].

IO-MNPs have been used as theragnostic agents because of two main interesting properties: their superparamagnetism [13,14] which allows them to be directed and localized to a target organ by using external magnetic force [15] and their excellent biocompatibility [16,17].

Klein et al. [18] have been reported that the uptake of IO-MNPs by MCF7 cells increased the radiosensitivity of kilovoltage energy by increasing the production of ROS.

Recently, the radiosensitivity of IO-MNPs has been approved in the presence of megavoltage energy [6,12,19]. The tendency for agglomeration due to high surface energy powerful magnetic attractions between particles and the van der Waals force is one of the obstacles that hinders the use of MNPs in medical applications [20]. So, Coating IO-MNPs by a biocompatible material makes them hydrophilic, compatible to bio-environments, functionalized and increases their stability [21–23].

* Corresponding author at: Biophysics Department, Faculty of Science, Cairo University, Giza, Egypt.
E-mail address: hfahmy@sci.cu.edu.eg (H.M. Fahmy).

https://doi.org/10.1016/j.lfs.2019.116756
Received 10 July 2019; Received in revised form 9 August 2019; Accepted 12 August 2019
Available online 13 August 2019
0024-3205/

Silica is considered as one of the most ideal coats for IO-MNPs [24–26]. The inner magnetic iron oxide core supplies the nanoparticles with magnetic properties, while the outer silica shell shows high chemical stability and biocompatibility [26,27].

Arvand et al. [28] tested silica-Coated IO-MNPs as a detector for sunset in food samples. Fudimura et al. [29] prepared and characterized methylene blue (MB)-containing silica-coated IO-MNPs and examined their impact on photodynamic therapy.

Silica nanoparticles have been reported as a radiosensitizer through the enhancing the mitochondrial ROS production [30] which means that using of Silica nanoparticles as a coat for IO-MNPs may facilitate their radiotherapeutic impact.

Although most of the previous research works were focused on the preparation of silica-coated magnetite nanoparticles (SIO-MNPs), yet there is still a lack of reports discussing their medical applications.

Up to the authors' knowledge, this is the first study on the evaluation of the radio sensitizing effect of silica-coated iron oxide nanoparticles SIO-MNPs. The aim of the present work is to synthesize SIO-MNPs and to investigate their radiotherapeutic impact on cancerous cell radiosensitivity using electron therapy.

2. Materials and methods

2.1. Materials

Iron (III) chloride hexahydrate ($FeCl_3{\cdot}6H_2O$), Iron (II) chloride tetrahydrate ($FeCl_2{\cdot}4H_2O$), 28% w/v % ammonia hydroxide solution, Tetraethyl orthosilicate (TEOS), trypsin, 10% fetal bovine serum (FBS), RPMI-1640 medium, L-glutamine, penicillin, streptomycin,3-(4,5-dimethylthiazol-2-yl) 2,5diphenyl tetrazolium bromide (MTT), Tris-borate- EDTA (TBE), EtBrstain, Phosphate buffered saline (PBS), dimethyl sulphoxide (DMSO), and 70% (v/v) ethanol were purchased from Sigma-Aldrich (Germany). MCF7; the human epithelial breast carcinoma cell lines (ATCC®: HTB-22™) was imported from ATCC (The American Type Culture Collection; Manassas, VA, USA) via Vacsera (the holding company for biological products and vaccines; Cairo, Egypt).

2.2. Methods

2.2.1. Preparation of IO-MNPs nanoparticles

IO-MNPs were prepared using the co-precipitation method of Lu et al. [31] and Elbialy et al. [32] with some modifications. Briefly, 0.01 M of $FeCl_2{\cdot}4H_2O$ and 0.02 M of $FeCl_3{\cdot}6H_2O$ were dissolved in 80 mL of deionized water with vigorous mechanical stirring. Then, 10 mL of ammonia solution (28 wt%) was dropwise added, and the reaction was maintained over stirrer at 80 °C for 30 min. Finally, a permanent magnet was used to separate the black precipitates (IO-MNPs) which were washed several times with deionized water and ethanol to remove the unreacted chemicals.

2.2.2. Preparation of silica-coated iron oxide nanoparticles (SIO-MNPs)

Coating of IO-MNPs surface with silica shell was obtained as follows: 100 mg of IO-MNPs was dispersed in ethanol deionized water solution (4: 1, v/v) by ultrasonication for 15 min. Then, 4.6 mL of ammonia solution (28 wt%) and 2 mL of TEOS were added into the above solution with vigorous stirring. The reaction proceeded at room temperature for 24 h with continuous stirring. The resultant product was washed several times with ethanol and deionized water and dried in an oven at 80 °C for 10 h [28].

2.2.3. Characterization of the IO-MNPs and SIO-MNPs

Morphological information of nanoparticles was examined using a transmission electron microscope (TEM) (JEM 1230 electron microscope. Jeol, Tokyo, Japan). A drop of solution was applied to a copper-coated carbon grid. In addition, a filter was used to draw the sample and the grid was left 5 min to dry at room temperature before the examination began. Dynamic light scattering (DLS) was used for measuring the size distribution of nanoparticles and molecules in suspension. The size measured by DLS was determined as hydrodynamic diameter (NP core together with a layer of surface-bound solvent). The size distribution and the surface potential of IO-MNPs and SIO-MNPs were investigated using Zeta Potential/Particle Seizer (NICOMP TM 380 ZLS, USA). The surface topography, shape and roughness of IO-MNPs and SIO-MNPs have been obtained using the atomic force microscope (AFM) (Wet – SPM9600. Japan). In AFM, the sample is scanned by a tip, during the scanning process, the force between the tip and the sample is evaluated by observing the cantilever deflection installed on the top of the tip. The deflection of the cantilever versus its location on the sample, produced a topographic picture of the sample [33].

Vibrating sample magnetometer (VSM) has been used to evaluate the saturation of magnetization (Ms) of IO-MNPs and SIO-MNPs (LakeShore 7410, LakeShore, and Westerville, USA).

2.2.4. Cell culture and irradiation setup

MCF-7 cells were grown in RPMI-1640 medium supplemented with 10% FBS, L-glutamine, penicillin, and streptomycin and were incubated at 37 °C in a humidified 5% CO_2 sterile incubator. Cell plates were exposed to electron beam using the linear accelerator (600C DBX, Varian, USA) operating at 6 MeV, the source-to-surfaces distance was adjusted at 100 cm for the irradiated culture plates at a radiation field size of 14 × 14 cm^2 [34].

2.2.5. MTT assay

MCF7 cells were cultured in 96 well plates (10^4 cells/well) and lifted for 48 h for attaching. After that MCF7 cells have been incubated with different concentrations (0, 5, 10, 20, 40 and 80 μg/ml) of IO-MNPs and SIO-MNPs. After 24 h, the cells were irradiated with different radiation doses (0, 0.5, 1, 2 and 4 Gy) and incubated at 37 °C. 24 h after irradiation, the cell viability % was assessed using MTT assay by incubating the cells for 2 h in a medium containing 0.5% MTT stain (25 μl/well). The developed intracytoplasmic MTT formazan crystals were dissolved using 0.05 ml DMSO for 30 min on a plate shaker. Optical densities (OD) were read at a wavelength of 570 nm using an ELISA plate reader (Biotek 8000; USA(.Viability percentage was calculated as follows: Cell viability percentage = (OD of treated cells / OD of untreated cells) × 100% [35]. Dose enhancement factor (DEF) values were obtained by dividing the viability of the cells exposed to radiation only by that of cells treated with the prepared nanoparticles and exposed to the same dose [12].

2.2.6. Revelation of DNA damage by using single cell gel electrophoresis assay (Comet assay)

The Comet assay was used to quantify the DNA damage induced by IO-MNPs and SIO-MNPs by estimating three different parameters: tail length, the percentage of DNA in the tail and the tail moment. MCF7 cells were cultured in two (6 well) plates, cells were counted (50,000 cells/well), and were treated with IO-MNPs and SIO-MNPs at concentrations of 10 and 40 μg/ml.

The first plate which would be exposed to 0.5 Gy, was divided to five groups: 0.5G1 is the control (untreated) group of cells, 0.5G2 is the group of cells that was treated with 10 μg/ml of IO-MNPs, 0.5G3 is the group of cells which was treated with 10 μg/ml of SIO-MNPs, 0.5G4 is the group of cells that was treated with 40 μg/ml of IO-MNPs and 0.5G5 is the group of cells which was treated with 40 μg/ml of SIO-MNPs. The second plate which would be exposed to 1 Gy, was divided to five groups: 1G1 is the control (untreated) group of cells, 1G2 is the group of cells that was treated with 10 μg/ml of IO-MNPs, 1G3 is the group of cells that was treated with 10 μg/ml of SIO-MNPs, 1G4 is the group of cells that was treated with 40 μg/ml of IO-MNPs and 1G5 is the group of cells that was treated with 40 μg/ml of SIO-MNPs.

After 24 h treatment, the cells were exposed to an electron beam at

doses of 0.5 and 1 Gy. The irradiated plates were then incubated for 24 h, after that, cells were treated with trypsin, centrifuged and washed with PBS and re-suspended in 100 μL of PBS. A mixture of 50 μL of the cell suspension and 500 μL of melted LM Agarose was formed and then, 75 μL was pipetted onto a pre-warmed comet slide and spread completely over the sample area.

At 4 °C, the slides were placed flat in the dark for 10 min to allow mixture solidification and then, submerged for 40 min into a pre-chilled lysis solution. The slides were placed in an alkaline medium for 40 min at room temperature in dark after being removed from lysis solution and washed twice for 5 min with Tris-Borate-EDTA (TBE).

The slides were electrophoresed at low voltage (300 mA, 25 V, 4 °C) for 20 min and then, placed in 70% ethanol for 5 min, removed, tapped, and air-dried overnight, after that, they were stained with EtBrstain designed for comet assay and allowed to air dry at room temperature for 6 h. Fluorescence-stained comet images were captured with a CCD camera (Optika vision pro, Italy) attached to the fluorescent microscope (Nikon ECLIPSE E600, Japan) and linked to a comet assay software program, comet score, version 5.0 which counted the tail length, percentage of DNA in tail and tail moment averages from 100 cells per sample.

2.2.7. Statistical analysis

Data were obtained from at least three independent experiments and were explicit as mean ± SD.

Using SPSS, one-way Analysis of Variance (ANOVA) was performed for the comet assay. Scheffe's test at statistically significant values ($p < 0.05$) was performed as the post hoc comparisons for independent and dependent groups.

3. Results

3.1. Characterization of IO-MNPs and SIO-MNPs

Dynamic light scattering assessments results showed that the average particle sizes of IO-MNPs and SIO-MNPs were 18.17 ± 4.5 nm and 164.18 ± 16.1 nm, respectively (Fig. 1[A]). In addition, the polydispersity index (PDI) values were 0.219 and 0.439 for IO-MNPs and SIO-MNPs, respectively.

Zeta potential measurements showed that the net surface charges of the prepared NPs were negative with an average value of −32 ± 1.8 and −41 ± 2.3 mv for the prepared IO-MNPs and SIO-MNPs, respectively.

The ultrastructure of the prepared nano-formulations is shown in Fig. 2[A, B]. Fig. 2[A] demonstrates the spherical shape of IO-MNPs with a mean diameter of 13.63 ± 1.36 nm. TEM micrograph of silica-coated magnetic nanoparticles particles (Fig. 2[B]) represents a spherical core-shell structure with a mean core diameter of 54.9 ± 10.1 nm, and the silica layers are about 43.35 ± 2 nm in thickness. As seen in the figure, the silica coat was assembled as a multi-layered pattern, in addition, the uniformity of silica coating thickness can be seen.

The surface morphology of IO-MNPs and SIO-MNPs has been investigated using AFM (Fig. 2[C, D]). Direct observation of atomic force microscopy images revealed that many small cavities were uniformly distributed on the IO-MNPs surface (Fig. 2[C]), while Fig. 2[D]) demonstrates the granular surface of SIO-MNPs. Surface roughness was found to be 1.878 ± 0.03 nm for IO-MNPs and 2.489 ± 0.12 nm for SIO-MNPs. The particle size extracted from AFM data was 15.6 ± 3.5 nm in the case of IO-MNPs and 152.3 ± 8.9 nm in the case of SIO-MNPs.

The magnetic properties of IO-MNPs and SIO-MNPs were characterized using VSM. The hysteresis loops of IO-MNPs and SIO-MNPs measured at room temperature as the function of the magnetic field are shown in Fig. 1[B]. The saturation magnetization (M_s) values of IO-MNPs and SIO-MNPs were 0.57 and 0.39 emu/cm^3 respectively. Also,

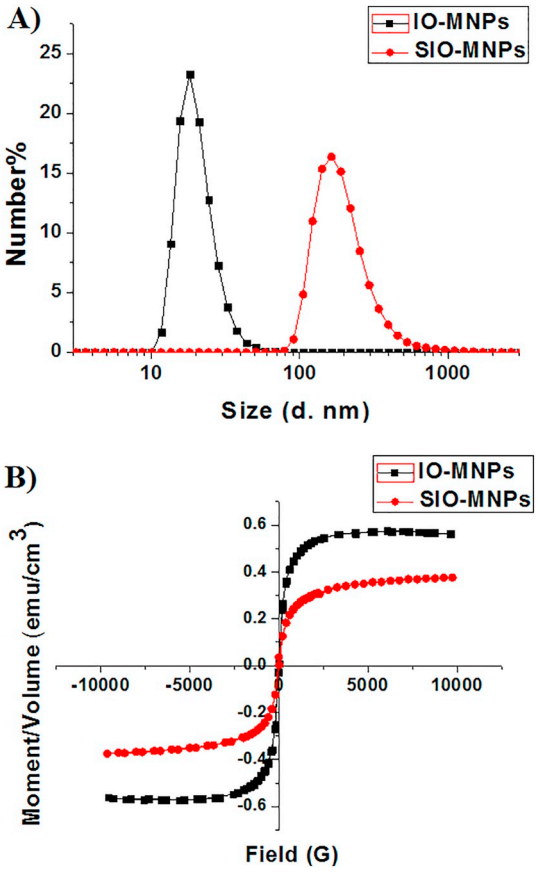

Fig. 1. (A) Particle size distribution of IO-MNPs and SIO-MNPs, (B) magnetization curves of IO-MNPs and SIO-MNPs.

IO-MNPs and SIO-MNPs exhibited a superparamagnetic behavior as no remanence in their hysteresis loops was observed.

3.2. In vitro experiments

3.2.1. Cell viability assay (MTT assay)

MTT assay was used to assess the radiosensitizing effect of IO-MNPs and SIO-MNPs against MCF7 breast cancer cell line. Fig. 3A–E shows the survival curves which illustrated the radiation effects on cancer cells incubated with different concentrations of IO-MNPs and SIO-MNPs (0, 5, 10, 20, 40 and 80 μg/ml). The results showed that the viability of cells treated with radiation only at doses of 0.5, 1, 2 and 4 Gy are 80%, 60%, 50%, and 47%, respectively (Fig. 3A). On the other hand, the incubation of cancerous cells with different concentrations of IO-MNPs, 24 h post irradiation, enhanced the damaging effects of radiation compared to cells treated with radiation only (Fig. 3B–F).

At lower doses (0.5 and 1 Gy), the viability of the cells treated with different concentrations of IO-MNPs dramatically decreased with increasing the concentration compared to cells treated with radiation only. The dose enhancement factor (DEF) values of the cells treated with different concentrations (5, 10, 20, 40 and 80 μg/ml) of IO-MNPs and exposed to 0.5 Gy were 1.08, 1.12, 1.23, 1.37 and 1.64, respectively.

In contrast, at higher exposure doses (2 and 4 Gy), there was no significant effect of concentration variation of IO-MNPs and the DEF values of cells treated with different IO-MNPs concentrations (5, 10, 20, 40 and 80 μg/ml) and exposed to 4 Gy were 1, 1.12, 1.11, 1.16 and 1.20, respectively.

For SIO-MNPs, cell viability results showed that, at low doses (0.5 and 1 Gy), the viabilities of MCF7 cells treated with 5, 10, 20, 40 and 80 μg/ml of SIO-MNPs decreased by about 25% than cells treated with

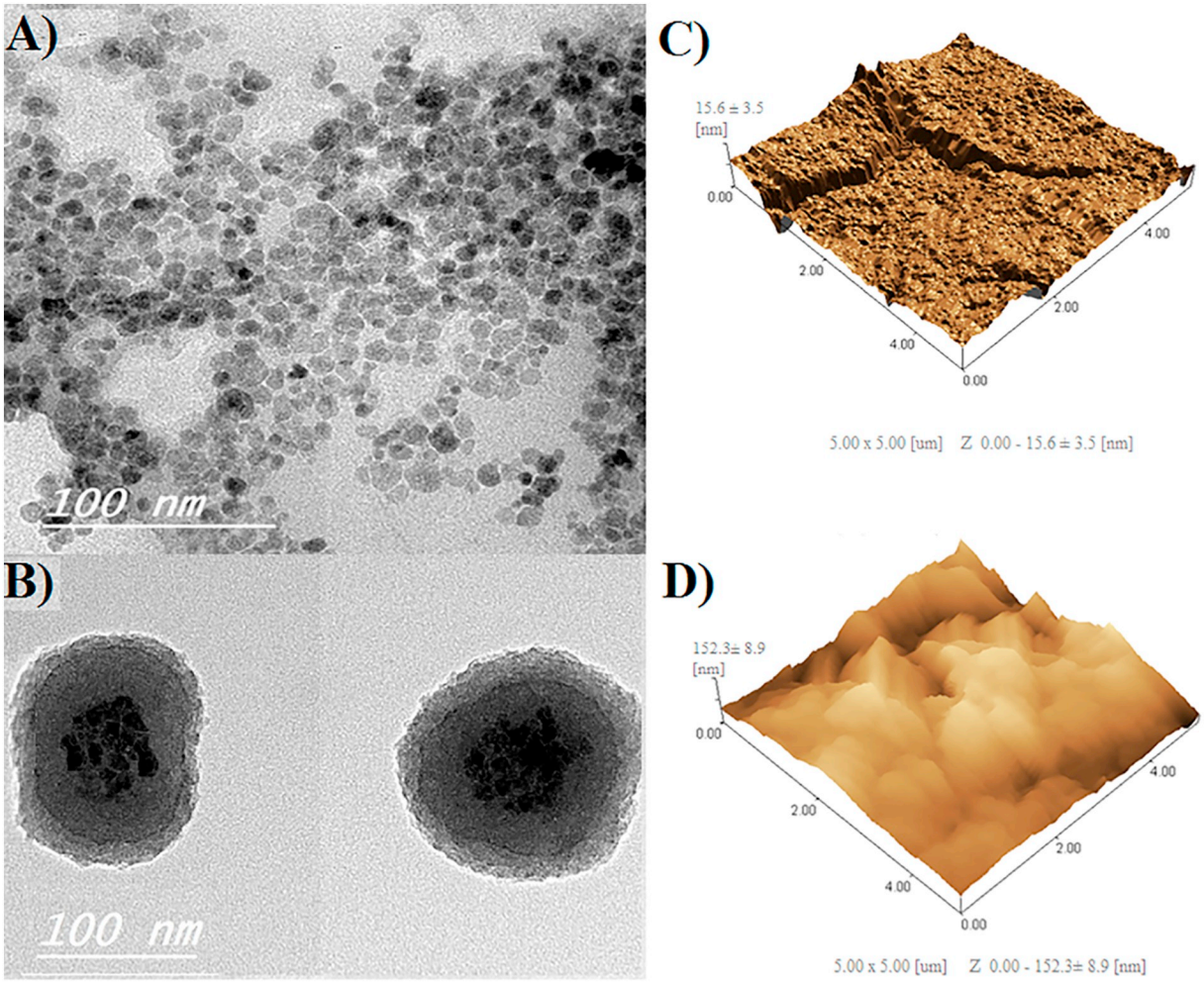

Fig. 2. (A) TEM image of IO-MNPs, (B) TEM image of SIO-MNPs, (C) AFM image of IO-MNPs, (D) AFM image of SIO-MNPs.

IO-MNPs with the same concentrations. This improvement in radiosensitizing effects extended to higher doses. For example, at 4 Gy, MCF7 cells treated with 5, 10, 20, 40 and 80 μg/ml of SIO-MNPs had DEF values of 1.03, 1.32, 1.29, 1.42 and 1.64, respectively. These were, in average, about 1.3-folds greater than that of cells treated with the same concentrations of IO-MNPs.

In the survival curve, the optimum concentration of SIO-MNPs was 80 μg/ml.

Table 1 shows that DEF values, which reflected the effect of IO-MNPs and SIO-MNPs as dose modifiers. DEF increased with increasing the concentration of IO-MNPs and SIO-MNPs and decreased with increasing the radiation dose. Overall, at each dose and concentration, DEF of SIO-MNPs was about 1.3-folds greater than that of IO-MNPs.

The obtained data confirmed that there was an improvement in the radiotherapeutic effect of SIO-MNPs over IO-MNPs.

3.2.2. Revelation of DNA damage by comet assay

Comet assay was used to assess the radiosensitizing and consequently the DNA damaging effect of IO-MNPs and SIO-MNPs against MCF7 cells. Fluorescence-stained comet images, tail length, % DNA in the tail and tail moment parameters were used to investigate the DNA degradation (Figs. 4 & 5).

Fluorescence-stained comet images showed that DNA damage was a concentration-dependent, as the damaging effect increased with increase in concentration (Figs. 4A & 5A). % DNA in tail and tail moment parameters of 0.5G3 and 1G3 were very close to that of 0.5G4 and 1G4, respectively. There were highly significant differences in % DNA in tail and tail moments of 0.5G5 and 1G5 compared to other groups (Figs. 4B & 5B). DNA damage is dose-dependent, as the damaging effect increases with increasing the radiation dose. The tail moment of 0.5G5 was 0.43 and increased to 5.8 for 1G5.

4. Discussion

In the present study, a series of methods are employed to investigate/or properly evaluate the properties of the prepared nanoparticles. DLS technique is used to determine the mean hydrodynamic diameter of nano-sized particles [36]. The average sizes of both IO-MNPs and SIO-MNPs as obtained by DLS is found to be larger than that determined using TEM (which is known to yield the exact size of the nanostructures) [37].These differences originate from the fact that DLS measures a particle's hydrodynamic diameter (main particle size + hydration shell) in aqueous environments and this measurement can be influenced by particle agglomeration [38] and the hydrodynamic conditions [39]. TEM images prove that the silica coating layer can act as a supporting substrate to prevent the aggregation of IO-MNPs. It well demonstrates the core–shell structure of the prepared SIO-MNPs.

The polydispersity index (PDI) is used to describe the degree of homogeneity of nanoparticles size distribution [40]. The PDI values ranging from 0.1 to 0.25 indicate a narrow size distribution, while a PDI > 0.5 is related to a broad distribution [41]. In the present work, the prepared IO-MNPs and SIO-MNPs have PDI value of 0.219 and 0.439, respectively. This indicates a narrow size distribution (homogenous distribution) of IO-MNPs and a slightly broad size distribution of

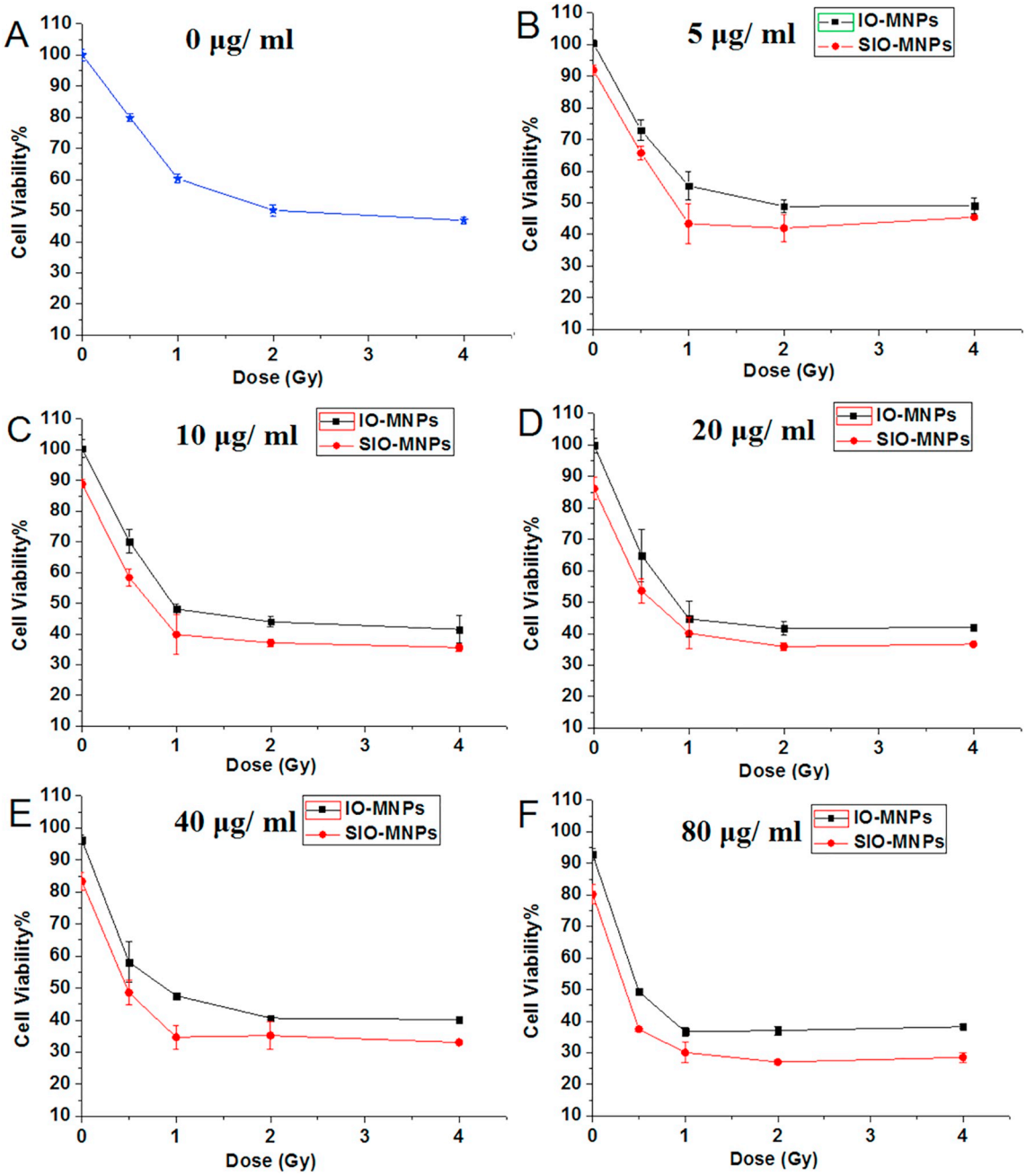

Fig. 3. Survival curves (A–F) of MCF-7 cells treated with different concentrations (0, 5, 10, 20, 40 and 80 µg/ml, respectively) of IO-MNPs and SIO-MNPs and exposed to different radiation doses (0, 0.5, 1, 2 and 4 Gy).

Table 1
Dose enhancement factor (DEF) values from the MTT assay for the MCF7 cell line. The cells incubated with IO-MNPs and SIO-MNPs (5, 10, 20, 40, 80 µg/ml concentrations) and irradiated with 6 MeV electron beam (0.5, 1, 2, 4 Gy).

Dose (Gy)	Dose enhancement factor (DEF)									
	Concentration (µg/ml)									
	IO-MNPs					SIO-MNPs				
	5	10	20	40	80	5	10	20	40	80
0.5	1.08	1.12	1.23	1.37	1.64	1.22	1.37	1.49	1.64	2.13
1	1.10	1.25	1.34	1.26	1.62	1.39	1.51	1.50	1.74	2.00
2	1.02	1.14	1.20	1.29	1.35	1.19	1.35	1.39	1.46	1.85
4	0.96	1.10	1.11	1.16	1.20	1.03	1.32	1.29	1.42	1.64

SIO-MNPs.

AFM can be used to measure the size of nanoparticles because the height (z-axis) of nanoparticles is considered representative of its real size and AFM measurements of distances in the z-axis are directly related to the real height of structures [42]. The size obtained from the AFM correlates well with the TEM results.

It was reported that the Silica coating is a multi-layered pattern with a uniform thickness and that the shape and thickness of the silica coat could be controlled by changing the reaction time and/or the concentration of the TEOS solution [43].

Zeta potential is the potential difference between liquids and solids across phase boundaries. It can influence: cellular uptake and intracellular trafficking of nanomaterials [44], regulate the selective adsorption of nanoparticles [45], plasma protein binding [46] and blood brain barrier integrity [47]. Also, the colloidal stability of any

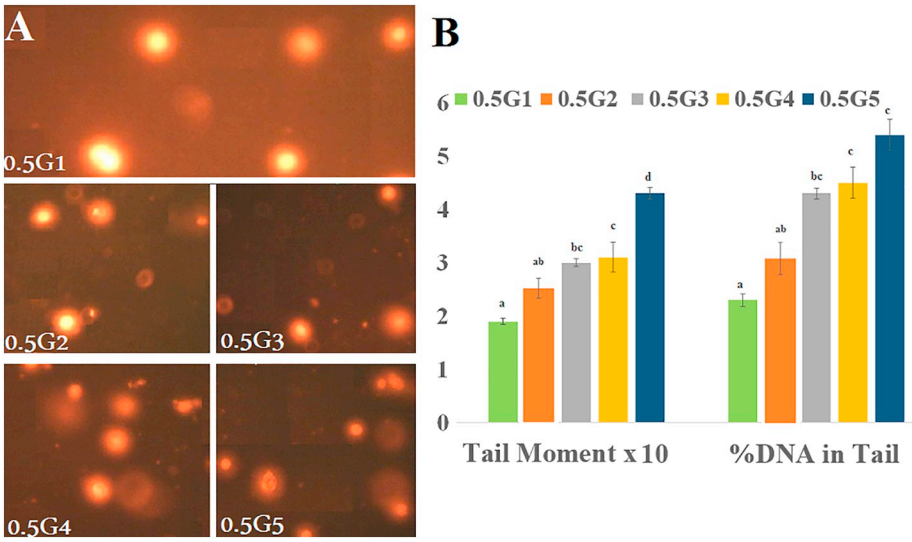

Fig. 4. (A) Fluorescence-stained comet images of MCF7 cells which were exposed to an electron beam at a dose of 0.5 Gy, (B) DNA damage of MCF7 cells assessed by the Comet assay for 0.5G1 (control, untreated group) and treated groups: 0.5G2 (10 μg/ml of IO-MNPs), 0.5G3 (10 μg/ml of SIO-MNPs), 0.5G4 (40 μg/ml of IO-MNPs) and 0.5G5 (40 μg/ml of SIO-MNPs). All groups were exposed to X ray photon beam at dose of 0.5 Gy. Different characters indicate significant ($p < 0.05$) different means.

nanoparticle's suspension depends on their zeta potential. At high positive or negative zeta potentials > 30 mV, the nanoparticles tend to repel each other and to create dispersion stability. If the particles are having low zeta potential values (smaller than 5 mV), there is no force to prevent the particles from agglomerating leading to dispersion instability [48,49].

Zeta potential measurements show that the net surface charge of IO-MNPs is negative. This is due to the presence of FeO^- group on IO-MNPs surface [50]. The silica coating layers enhance the stability of IO-MNPs as it increases the surface negative charge. SIO-MNPs surface negative charge is due to deprotonation of silanol group (SiO^-) [51,52].

The Magnetic properties of the IO-MNPs and SIO-MNPs are investigated using VSM, the hysteresis loops of IO-MNPs and SIO-MNPs demonstrate the superparamagnetic behavior as the Retentivity (M_r) and the coercivity are close to zero [53]. The saturation magnetization (M_s) values of IO-MNPs and SIO-MNPs are 0.57 and 0.38804 emu/cm^3, respectively. These results indicate that silica coating layer do not destruct the superparamagnetic behavior of IO-MNPs and the composite can be easily recovered by magnetic separation. SIO-MNPs hold great promise as a magnetic resonance imaging (MRI) contrast agent.

Cell viability results demonstrate that there is no significant change in the cell viability after incubation with different concentrations of IO-MNPs and SIO-MNPs which indicates biocompatible features of the prepared nano-formulations. It was assumed that biocompatible materials have a cell viability of > 80% [54]. But without irradiation, SIO-MNPs show higher potent effect against breast cancerous cells compared to IO-MNPs with a concentration-dependent pattern. This may be attributed to that the silica coating layer facilitates the cellular uptake by increasing the cellular binding capability through its rough surface [55].

Treatment of tumor cells with MeV electron beam is associated with one of electron interactions either ionization or radiative losses. In ionization, energy lost is generally deposited in the instant area but for radiative losses energy lost can propagate outmost before it is absorbed as it produces photon inside the cells [56]. Through collisional ionization and ensuing Auger cascades, electrons can activate electron emission from high-Z nanoparticles, leading to generate the secondary electrons which cause excitation and ionization of the surrounding biomolecules and the production of ROS [57]. The portion of electron radiative loss increases with the presence of high Z NPs which increase the cell killing due to enhancing ROS production [58].

After irradiation process (using MeV electrons), results show that IO-MNPs improve the potent effect of electrons radiotherapy. There is significant viability reduction for cells treated with IO-MNPs compared to those treated with radiation only. Also, it is found that the

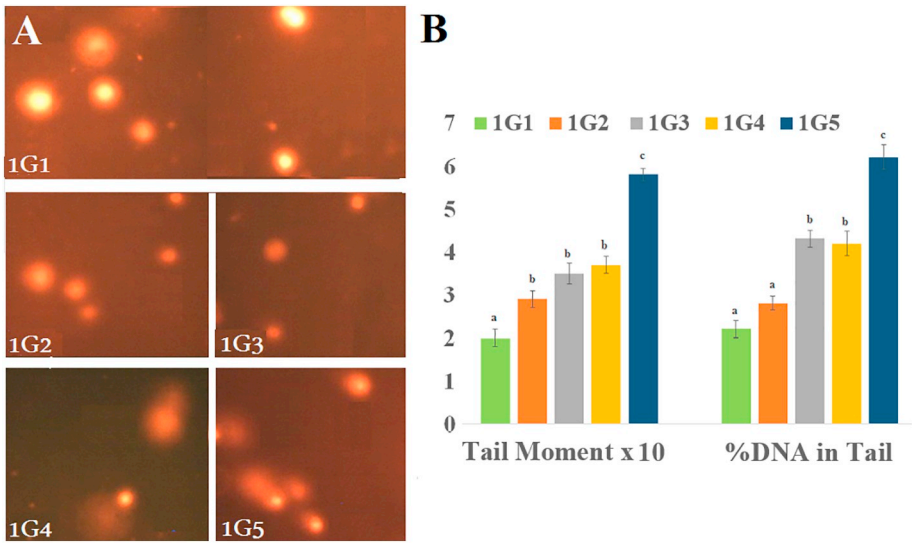

Fig. 5. (A) Fluorescence-stained comet images of MCF7 cells which were exposed to an electron beam at a dose of 1 Gy, (B) DNA damage of MCF7 cells assessed by the Comet assay for 1G1 (control, untreated group) and treated groups: 1G2 (10 μg/ml of IO-MNPs), 1G3 (10 μg/ml of SIO-MNPs), 1G4 (40 μg/ml of IO-MNPs) and 1G5 (40 μg/ml of SIO-MNPs). All groups were exposed to X ray photon beam at dose of 1 Gy. Different letters indicate significant ($p < 0.05$) different means.

radiosensitizing effect of IO-MNPs is concentration dependent. This may be due to an increase in the concentration of nanoparticles in cells leading to an increase in the cellular internalization which leads to the decrease in the cell survival percentage due to increasing the probability of the photoelectric interaction occurrence within the cells because of high effective atomic number [59].

Interestingly, in general, the results demonstrate more potent radiosensitizing effects and higher dose enhancement factors of SIO-MNPs over IO-MNPs against MCF7 cancer cells. This may be attributed to: (1) Surface roughness which play an important role in cellular internalization, as mentioned previously that the surface roughness of SIO-MNPs is about 1.3-folds greater than that of IO-MNPs, and so the cellular internalization of SIO-MNPs will be more than IO-MNPs. From the practical point of view, this finding enables us to reduce the given dose of radiation by about 30% when using SIO-MNPs as radiosensitizers (this is a great advantage). Also, these results proved that the presence of silica coat didn't degrade the radio-sensitization effect of IO-MNPs. The strength of nanoparticle-cell interactions, cell adhesion promotion [60] and the enhancement of cellular uptake [61,62] instructed by surface coarseness. It has been demonstrated that surface roughness of nanoparticles enhances the biomolecules binding and cellular uptake due to increased surface area which will imply a larger adsorbed amount. Also, changing the surface roughness may alter the interaction potentials between the nanoparticle and the adsorbing molecules [63]. (2) The increased ROS production induced by radiation into cells treated with SIO-MNPs in comparison to those treated with IO-MNPs. Silica nanoparticles were reported as a radiosensitizer through enhancing ROS production in cancer cells [18].

In tumor cells, iron oxide nanoparticles stimulate the generation of ROS. Immediate chelation by adenosine phosphate may be occurring by the iron ions released into the cytosol and the formation of the highly reactive OH· may be catalyzed by the participation of the chelated iron ions in the Haber–Weiss chemistry which causes cellular membranes, proteins and DNA damage [64–67]. The reaction of these free radicals with biomolecules can lead to single-strand breaks (SSBs) or double-strand breaks (DSBs) of DNA and cross-linking of DNA–DNA or DNA–protein, resulting in cell apoptosis which is indicated as indirect effect of ionizing radiation [68]. The hydroxyl ion is considered as being a major source of cellular damage by lipid peroxidation. The interaction with lipid bilayers also increases membrane permeability [69].

The comet assay is performed to illustrate the effect of electron beam combined with the prepared NPs against the DNA of MCF7 cells. DNA damage can be represented by measuring %DNA in tail and tail moment parameters.

Comet assay demonstrates that, as the radiation dose and the concentration of NPs increase, the amount of DNA (for the treated MCF7 cells) migrates more rapidly towards the anode compared to cell treated with radiation. This represents an increase in the degree of DNA damage. Interestingly, it is found that cells treated with SIO-MNPs and exposed to radiation exhibit more DNA damage than those treated with IO-MNPs.

The group of cells treated with 40 μg/ml SIO-MNPs and exposed to 0.5 Gy and 1Gy shows a highly significant DNA damage compared to other groups. This indicates larger number of DNA double-strand breaks which may be due to high production of ROS [70].

With different doses, the DNA damage of MCF7 cells treated with 10 μg/ml of SIO-MNPs exhibit more DNA damage than those treated with 10 μg/ml of IO-MNPs which indicates increased SIO-MNPs internalization and ROS production into cells in comparison with IO-MNPs. Also, cells treated with 10 μg/ml SIO-MNPs show very close results compared to cells treated with 40 μg/ml IO-MNPs. This indicates that low concentrations of SIO-MNPs can produce the same fraction of ROS as the higher concentrations of IO-MNP. This may be due to an increase in SIO-MNPs internalization and ROS production into cells in comparison with IO-MNPs.

It can be stated that this is the first study on the radio sensitizing effect of SIO-MNPs, the present study revealed some interesting properties of this multifunctional nanoparticle. If SIO-MNPs would be used as a radiosensitizer during radiotherapy, it can also be used as a contrast agent in MRI. On other word, SIO-MNPs can be used as theragnostic agent in cancer therapy.

5. Conclusion

Based on the characteristic results, we can declare that IO-MNPs and SIO-MNPs were successfully synthesized. SIO-MNPs can be used as a multifunctional nano-platform. Silica coating layer do not destruct the superparamagnetic behavior of IO-MNPs and the composite can be easily recovered by magnetic separation. SIO-MNPs hold great promise as MRI contrast agent.

Silica layer not only enhanced the stability of IO-MNPs but also enhanced the radiosensitizing effect by increasing ROS generation. The characteristic of radiosensitization was examined for IO-MNPs and SIO-MNPs by using MTT and comet assays. The results proved that when SIO-MNPs were combined with the radiation, the lower doses had the same potent effect as the higher doses do without these nanoparticles. This will have the advantage of reducing the dose of healthy tissues during the treatment. The effect of SIO-MNPs as radiosensitizers was highly significant comparing to IO-MNPs.

Therefore, the SIO-MNPs nanostructure would hold great promise as a novel radiosensitizer. Further, in vivo results are still required.

Funding sources

No funding sources.

Declaration of competing interest

No conflict of interest.

References

[1] F. Li, Z. Liang, J. Liu, J. Sun, X. Hu, M. Zhao, J. Liu, R. Bai, D. Kim, X. Sun, T. Hyeon, Dynamically reversible Iron oxide nanoparticle assemblies for targeted amplification of T1-weighted magnetic resonance imaging of tumors, Nano Lett. (2019), https://doi.org/10.1021/acs.nanolett.8b04411.

[2] A. Jemal, F. Bray, M.M. Center, J. Ferlay, E. Ward, D. Forman, Global cancer statistics, CA Cancer J. Clin. 61 (2) (2011) 69–90, https://doi.org/10.3322/caac.20107.

[3] H.D. Nelson, B. Zakher, A. Cantor, R. Fu, J. Griffin, E.S. O'meara, D.S. Buist, K. Kerlikowske, N.T. van Ravesteyn, A. Trentham-Dietz, J.S. Mandelblatt, Risk factors for breast cancer for women aged 40 to 49 years: a systematic review and meta-analysis, Ann. Intern. Med. 156 (9) (2012) 635–648, https://doi.org/10.1059/0003-4819-156-9-201205010-00006.

[4] P.P. Connell, S. Hellman, Advances in radiotherapy and implications for the next century: a historical perspective, Cancer Res. 69 (2) (2009) 383–392, https://doi.org/10.1158/0008-5472.CAN-07-6871.

[5] D. Eriksson, T. Stigbrand, Radiation-induced cell death mechanisms, Tumor Biol. 31 (4) (2010) 363–372, https://doi.org/10.1007/s13277-010-0042-8.

[6] S. Jafari, M. Cheki, M.B. Tavakoli, A. Zarrabi, K.G. Sani, R. Afzalipour, Investigation of combination effect between 6 MV X ray radiation and polyglycerol coated superparamagnetic iron oxide nanoparticles on U87-MG cancer cells, Journal of Biomedical Physics and Engineering (2018), https://doi.org/10.31661/jbpe.v0i0.929.

[7] S. Khoei, S.R. Mahdavi, H. Fakhimikabir, A. Shakeri-Zadeh, A. Hashemian, The role of iron oxide nanoparticles in the radiosensitization of human prostate carcinoma cell line DU145 at megavoltage radiation energies, Int. J. Radiat. Biol. 90 (5) (2014) 351–356, https://doi.org/10.3109/09553002.2014.888104.

[8] A. Malik, M. Sultana, A. Qazi, M.H. Qazi, G. Parveen, S. Waquar, A.B. Ashraf, M. Rasool, Role of natural radiosensitizers and cancer cell radioresistance: an update, Anal. Cell. Pathol. 2016 (2016) 1–8, https://doi.org/10.1155/2016/6146595.

[9] M. Krause, A. Dubrovska, A. Linge, M. Baumann, Cancer stem cells: radioresistance, prediction of radiotherapy outcome and specific targets for combined treatments, Adv. Drug Deliv. Rev. 109 (2017) 63–73, https://doi.org/10.1016/j.addr.2016.02.002.

[10] R.V. Lalla, N. Treister, T. Sollecito, B. Schmidt, L.L. Patton, K. Mohammadi, J.S. Hodges, M.T. Brennan, OraRad Study Group, Oral complications at 6 months after radiation therapy for head and neck cancer, Oral Dis. 23 (8) (2017) 1134–1143, https://doi.org/10.1111/odi.12710.

[11] M. Rezaei, K. Khoshgard, L. Hosseinzadeh, A. Haghparast, M.T. Eivazi, Application of Dextran-coated Iron Oxide Nanoparticles in Enhancing the Radiosensitivity of Cancerous Cells in Radiotherapy With High-energy Electron Beams, (2019), https://doi.org/10.4103/jcrt.JCRT_19_17.
[12] H. Fakhimikabir, M.B. Tavakoli, A. Zarrabi, A. Amouheidari, S. Rahgozar, The role of folic acid-conjugated polyglycerol coated iron oxide nanoparticles on radiosensitivity with clinical electron beam (6 MeV) on human cervical carcinoma cell line: in vitro study, J. Photochem. Photobiol. B Biol. 182 (2018) 71–76, https://doi.org/10.1016/j.jphotobiol.2018.03.023.
[13] A. Petri-Fink, M. Chastellain, L. Juillerat-Jeanneret, A. Ferrari, H. Hofmann, Development of functionalized superparamagnetic iron oxide nanoparticles for interaction with human cancer cells, Biomaterials 26 (15) (2005) 2685–2694, https://doi.org/10.1016/j.biomaterials.2004.07.023.
[14] E.K. Schlachter, H.R. Widmer, A. Bregy, T. Lönnfors-Weitzel, I. Vajtai, N. Corazza, V.J. Bernau, T. Weitzel, P. Mordasini, J. Slotboom, G. Herrmann, Metabolic pathway and distribution of superparamagnetic iron oxide nanoparticles: in vivo study, Int. J. Nanomedicine 6 (2011) 1793, https://doi.org/10.2147/IJN.S23638.
[15] A. S Wadajkar, J. U Menon, T. Kadapure, R. T Tran, J. Yang, K. T Nguyen, Design and application of magnetic-based theranostic nanoparticle systems, Recent patents on biomedical engineering 6 (1) (2013) 47–57, https://doi.org/10.2174/1874764711306010007.
[16] A.S. Lübbe, C. Alexiou, C. Bergemann, Clinical applications of magnetic drug targeting, J. Surg. Res. 95 (2) (2001) 200–206, https://doi.org/10.1006/jsre.2000.6030.
[17] J.S. Kim, T.J. Yoon, K.N. Yu, B.G. Kim, S.J. Park, H.W. Kim, K.H. Lee, S.B. Park, J.K. Lee, M.H. Cho, Toxicity and tissue distribution of magnetic nanoparticles in mice, Toxicol. Sci. 89 (1) (2005) 338–347, https://doi.org/10.1093/toxsci/kfj027.
[18] S. Klein, A. Sommer, L.V. Distel, W. Neuhuber, C. Kryschi, Superparamagnetic iron oxide nanoparticles as radiosensitizer via enhanced reactive oxygen species formation, Biochem. Biophys. Res. Commun. 425 (2) (2012) 393–397, https://doi.org/10.1016/j.bbrc.2012.07.108.
[19] N.G. Shetake, A. Kumar, B.N. Pandey, Iron-oxide nanoparticles target intracellular HSP90 to induce tumor radio-sensitization, Biochimica et Biophysica Acta (BBA)-General Subjects 1863 (5) (2019) 857–869, https://doi.org/10.1016/j.bbagen.2019.02.010.
[20] A.H. Lu, E.E. Salabas, F. Schüth, Magnetic nanoparticles: synthesis, protection, functionalization, and application, AngewandteChemie International Edition 46 (8) (2007) 1222–1244, https://doi.org/10.1002/anie.200602866.
[21] F. Hu, K.G. Neoh, L. Cen, E.T. Kang, Cellular response to magnetic nanoparticles "PEGylated" via surface-initiated atom transfer radical polymerization, Biomacromolecules 7 (3) (2006) 809–816, https://doi.org/10.1021/bm050870e.
[22] O. Veiseh, C. Sun, J. Gunn, N. Kohler, P. Gabikian, D. Lee, N. Bhattarai, R. Ellenbogen, R. Sze, A. Hallahan, J. Olson, Optical and MRI multifunctional nanoprobe for targeting gliomas, Nano Lett. 5 (6) (2005) 1003–1008, https://doi.org/10.1021/nl0502569.
[23] W. Wu, Q. He, C. Jiang, Magnetic iron oxide nanoparticles: synthesis and surface functionalization strategies, Nanoscale Res. Lett. 3 (11) (2008) 397, https://doi.org/10.1007/s11671-008-9174-9.
[24] Z. Zhang, L. Zhang, L. Chen, L. Chen, Q.H. Wan, Synthesis of novel porous magnetic silica microspheres as adsorbents for isolation of genomic DNA, Biotechnol. Prog. 22 (2) (2006) 514–518, https://doi.org/10.1021/bp050400w.
[25] Z. Lu, J. Dai, X. Song, G. Wang, W. Yang, Facile synthesis of Fe3O4/SiO2 composite nanoparticles from primary silica particles, Colloids Surf. A Physicochem. Eng. Asp. 317 (1–3) (2008) 450–456, https://doi.org/10.1016/j.colsurfa.2007.11.020.
[26] M. Shahriary, H. Veisi, M. Hekmati, S. Hemmati, In situ green synthesis of Ag nanoparticles on herbal tea extract (Stachys lavandulifolia)-modified magnetic iron oxide nanoparticles as antibacterial agent and their 4-nitrophenol catalytic reduction activity, Mater. Sci. Eng. C 90 (2018) 57–66, https://doi.org/10.1016/j.msec.2018.04.044.
[27] E. Catalano, M. Miola, S. Ferraris, S. Novak, F. Oltolina, A. Cochis, M. Prat, E. Vernè, L. Rimondini, A. Follenzi, Magnetite and silica-coated magnetite nanoparticles are highly biocompatible on endothelial cells in vitro, Biomedical Physics & Engineering Express 3 (2) (2017) 025015, , https://doi.org/10.1088/2057-1976/aa62cc.
[28] M. Arvand, Z. Erfanifar, M.S. Ardaki, A new core@ shell silica-coated magnetic molecular imprinted nanoparticles for selective detection of sunset yellow in food samples, Food Anal. Methods 10 (7) (2017) 2593–2606, https://doi.org/10.1007/s12161-017-0803-8.
[29] K.A. Fudimura, A.B. Seabra, M.C. Santos, P.S. Haddad, Synthesis and characterization of methylene blue-containing silica-coated magnetic nanoparticles for photodynamic therapy, J. Nanosci. Nanotechnol. 17 (1) (2017) 133–142, https://doi.org/10.1166/jnn.2017.12715.
[30] S. Klein, M.L. Dell'Arciprete, M. Wegmann, L.V. Distel, W. Neuhuber, M.C. Gonzalez, C. Kryschi, Oxidized silicon nanoparticles for radiosensitization of cancer and tissue cells, Biochem. Biophys. Res. Commun. 434 (2) (2013) 217–222, https://doi.org/10.1016/j.bbrc.2013.03.042.
[31] F. Lu, H. Li, M. Sun, L. Fan, H. Qiu, X. Li, C. Luo, Flow injection chemiluminescence sensor based on core–shell magnetic molecularly imprinted nanoparticles for determination of sulfadiazine, Anal. Chim. Acta 718 (2012) 84–91, https://doi.org/10.1016/j.aca.2011.12.054.
[32] N.S. Elbialy, M.M. Fathy, W.M. Khalil, Preparation and characterization of magnetic gold nanoparticles to be used as doxorubicin nanocarriers, Physica Medica 30 (7) (2014) 843–848, https://doi.org/10.1016/j.ejmp.2014.05.012.
[33] H.J. Butt, B. Cappella, M. Kappl, Force measurements with the atomic force microscope: technique, interpretation and applications, Surf. Sci. Rep. 59 (1–6) (2005) 1–152, https://doi.org/10.1016/j.surfrep.2005.08.003.
[34] M.M. Fathy, F.S. Mohamed, N. Elbialy, W.M. Elshemey, Multifunctional chitosan-capped gold nanoparticles for enhanced cancer chemo-radiotherapy: an invitro study, Physica Medica 48 (2018) 76–83, https://doi.org/10.1016/j.ejmp.2018.04.002.
[35] A. Monks, D. Scudiero, P. Skehan, R. Shoemaker, K. Paull, D. Vistica, C. Hose, J. Langley, P. Cronise, A. Vaigro-Wolff, M. Gray-Goodrich, Feasibility of a high-flux anticancer drug screen using a diverse panel of cultured human tumor cell lines, JNCI: Journal of the National Cancer Institute 83 (11) (1991) 757–766, https://doi.org/10.1093/jnci/83.11.757.
[36] I. Sondi, B. Salopek-Sondi, Silver nanoparticles as antimicrobial agent: a case study on E. coli as a model for Gram-negative bacteria, J. Colloid Interface Sci. 275 (1) (2004) 177–182, https://doi.org/10.1016/j.jcis.2004.02.012.
[37] K.N. Han, N.S. Kim, Challenges and opportunities in direct write technology using nano-metal particles, KONA Powder and Particle Journal 27 (2009) 73–83, https://doi.org/10.14356/kona.2009009.
[38] R.C. Murdock, L. Braydich-Stolle, A.M. Schrand, J.J. Schlager, S.M. Hussain, Characterization of nanomaterial dispersion in solution prior to in vitro exposure using dynamic light scattering technique, Toxicol. Sci. 101 (2) (2008) 239–253, https://doi.org/10.1093/toxsci/kfm240.
[39] K. Takahashi, H. Kato, T. Saito, S. Matsuyama, S. Kinugasa, Precise measurement of the size of nanoparticles by dynamic light scattering with uncertainty analysis, Part. Part. Syst. Charact. 25 (1) (2008) 31–38, https://doi.org/10.1002/ppsc.200700015.
[40] M. El Gazzar, R. El Mezayen, J.C. Marecki, M.R. Nicolls, A. Canastar, S.C. Dreskin, Anti-inflammatory effect of thymoquinone in a mouse model of allergic lung inflammation, Int. Immunopharmacol. 6 (7) (2006) 1135–1142, https://doi.org/10.1016/j.intimp.2006.02.004.
[41] L. Wu, J. Zhang, W. Watanabe, Physical and chemical stability of drug nanoparticles, Adv. Drug Deliv. Rev. 63 (6) (2011) 456–469, https://doi.org/10.1016/j.addr.2011.02.001.
[42] M. Gracia-Pinilla, E. Martínez, G.S. Vidaurri, E. Pérez-Tijerina, Deposition of size-selected Cu nanoparticles by inert gas condensation, Nanoscale Res. Lett. 5 (1) (2010) 180, https://doi.org/10.1007/s11671-009-9462-z.
[43] Y. Yin, Y. Lu, Y. Sun, Y. Xia, Silver nanowires can be directly coated with amorphous silica to generate well-controlled coaxial nanocables of silver/silica, Nano Lett. 2 (4) (2002) 427–430, https://doi.org/10.1021/nl025508+.
[44] G. Buckton, Interfacial phenomena in drug delivery and targeting, CRC press (2000), https://doi.org/10.1201/9781482296785.
[45] A. Hoshino, K. Fujioka, T. Oku, M. Suga, Y.F. Sasaki, T. Ohta, M. Yasuhara, K. Suzuki, K. Yamamoto, Physicochemical properties and cellular toxicity of nanocrystal quantum dots depend on their surface modification, Nano Lett. 4 (11) (2004) 2163–2169, https://doi.org/10.1021/nl048715d.
[46] A. Pietroiusti, M. Massimiani, I. Fenoglio, M. Colonna, F. Valentini, G. Palleschi, A. Camaioni, A. Magrini, G. Siracusa, A. Bergamaschi, A. Sgambato, Low doses of pristine and oxidized single-wall carbon nanotubes affect mammalian embryonic development, ACS Nano 5 (6) (2011) 4624–4633, https://doi.org/10.1021/nn200372g.
[47] J.V. Georgieva, D. Kalicharan, P.O. Couraud, I.A. Romero, B. Weksler, D. Hoekstra, I.S. Zuhorn, Surface characteristics of nanoparticles determine their intracellular fate in and processing by human blood–brain barrier endothelial cells in vitro, Mol. Ther. 19 (2) (2011) 318–325, https://doi.org/10.1038/mt.2010.236.
[48] D. Paolino, M. Fresta, P. Sinha, I.M. Ferrar, Drug delivery systems, Webster JG (ed) Encyclopedia of Medical Devices and Instrumentation, 2nd edn, Wiley, New York, 2006, pp. 437–495, , https://doi.org/10.1002/0471732877.emd274.
[49] M. Gumustas, C.T. Sengel-Turk, A. Gumustas, S.A. Ozkan, B. Uslu, Effect of polymer-based nanoparticles on the assay of antimicrobial drug delivery systems, Multifunctional Systems for Combined Delivery, Biosensing and Diagnostics, 2017, pp. 67–108, , https://doi.org/10.1016/B978-0-323-52725-5.00005-8.
[50] A.L. Andrade, D.M. Souza, M.C. Pereira, J.D. Fabris, R.Z. Domingues, Synthesis and characterization of magnetic nanoparticles coated with silica through a sol-gel approach, Cerâmica 55 (336) (2009) 420–424, https://doi.org/10.1590/S0366-69132009000400013.
[51] A.A. Christy, P.K. Egeberg, Quantitative determination of surface silanol groups in silicagel by deuterium exchange combined with infrared spectroscopy and chemometrics, Analyst 130 (5) (2005) 738–744, https://doi.org/10.1039/B501895C.
[52] A.H. Lee, S.F. Gessert, Y. Chen, N.V. Sergeev, B. Haghiri, Preparation of iron oxide silica particles for Zika viral RNA extraction, Heliyon 4 (3) (2018) e00572, , https://doi.org/10.1016/j.heliyon.2018.e00572.
[53] Z. Li, M. Kawashita, N. Araki, M. Mistumori, M. Hiraoka, Effect of particle size of magnetite nanoparticles on heat generating ability under alternating magnetic field, Bioceram. Dev. Appl. 1 (2011) 1–4, https://doi.org/10.4303/bda/D110128.
[54] J. Zhang, Y. Wang, H. Ji, Y. Wei, N. Wu, B. Zuo, Q. Wang, Magnetic nanocomposite catalysts with high activity and selectivity for selective hydrogenation of ortho-chloronitrobenzene, J. Catal. 229 (1) (2005) 114–118, https://doi.org/10.1016/j.jcat.2004.09.029.
[55] Y. Niu, M. Yu, J. Zhang, Y. Yang, C. Xu, M. Yeh, ... C. Yu, Synthesis of silica nanoparticles with controllable surface roughness for therapeutic protein delivery, J. Mater. Chem. B 3 (43) (2015) 8477–8485, https://doi.org/10.1039/C5TB01405K.
[56] F.M. Khan, J.P. Gibbons, Three-dimensional conformal radiation therapy, in: G. Khan (Ed.), Khan's the Physics of Radiation Therapy, 5th edn, Lippincott Williams & Wilkins, Philadelphia, 2014, pp. 413–429.
[57] Z. Kuncic, S. Lacombe, Nanoparticle radio-enhancement: principles, progress and application to cancer treatment, Phys. Med. Biol. 63 (2) (2018) 1–27, https://doi.org/10.1088/1361-6560/aa99ce.
[58] W.N. Rahman, N. Bishara, T. Ackerly, C.F. He, P. Jackson, C. Wong, R. Davidson, M. Geso, Enhancement of radiation effects by gold nanoparticles for superficial

radiation therapy, Nanomedicine 5 (2) (2009) 136–142, https://doi.org/10.1016/j.nano.2009.01.014.
[59] K. Khoshgard, P. Kiani, A. Haghparast, L. Hosseinzadeh, M.T. Eivazi, Radiation dose rate affects the radiosensitization of MCF-7 and HeLa cell lines to X-rays induced by dextran-coated iron oxide nanoparticles, Int. J. Radiat. Biol. 93 (8) (2017) 757–763, https://doi.org/10.1080/09553002.2017.1321806.
[60] Y.S. Lin, C.L. Haynes, Impacts of mesoporous silica nanoparticle size, pore ordering, and pore integrity on hemolytic activity, J. Am. Chem. Soc. 132 (13) (2010) 4834–4842, https://doi.org/10.1021/ja910846q.
[61] C. LoPresti, M. Massignani, C. Fernyhough, A. Blanazs, A.J. Ryan, J. Madsen, N.J. Warren, S.P. Armes, A.L. Lewis, S. Chirasatitsin, A.J. Engler, Controlling polymersome surface topology at the nanoscale by membrane confined polymer/polymer phase separation, ACS Nano 5 (3) (2011) 1775–1784, https://doi.org/10.1021/nn102455z.
[62] Y. Niu, M. Yu, S.B. Hartono, J. Yang, H. Xu, H. Zhang, J. Zhang, J. Zou, A. Dexter, W. Gu, C. Yu, Nanoparticles mimicking viral surface topography for enhanced cellular delivery, Adv. Mater. 25 (43) (2013) 6233–6237, https://doi.org/10.1002/adma.201302737.
[63] K. Rechendorff, M.B. Hovgaard, M. Foss, V.P. Zhdanov, F. Besenbacher, Enhancement of protein adsorption induced by surface roughness, Langmuir 22 (26) (2006) 10885–10888, https://doi.org/10.1021/la0621923.
[64] J. Emerit, C. Beaumont, F. Trivin, Iron metabolism, free radicals, and oxidative injury, Biomed. Pharmacother. 55 (6) (2001) 333–339, https://doi.org/10.1016/S0753-3322(01)00068-3.
[65] A. Nel, T. Xia, L. Mädler, N. Li, Toxic potential of materials at the nanolevel, science 311 (5761) (2006) 622–627, https://doi.org/10.1126/science.1114397.
[66] M. Auffan, W. Achouak, J. Rose, M.A. Roncato, C. Chanéac, D.T. Waite, A. Masion, J.C. Woicik, M.R. Wiesner, J.Y. Bottero, Relation between the redox state of iron-based nanoparticles and their cytotoxicity toward Escherichia coli, Environmental science & technology 42 (17) (2008) 6730–6735, https://doi.org/10.1021/es800086f.
[67] M. Mahmoudi, A. Simchi, M. Imani, M.A. Shokrgozar, A.S. Milani, U.O. Häfeli, P. Stroeve, A new approach for the in vitro identification of the cytotoxicity of superparamagnetic iron oxide nanoparticles, Colloids Surf. B: Biointerfaces 75 (1) (2010) 300–309, https://doi.org/10.1016/j.colsurfb.2009.08.044.
[68] D.M. Sridharan, A. Asaithamby, S.M. Bailey, S.V. Costes, P.W. Doetsch, W.S. Dynan, A. Kronenberg, K.N. Rithidech, J. Saha, A.M. Snijders, E. Werner, Understanding cancer development processes after HZE-particle exposure: roles of ROS, DNA damage repair, and inflammation, Radiat. Res. 183 (1) (2015) 1–26, https://doi.org/10.1667/RR13804.1.
[69] D. Kwatra, A. Venugopal, S. Anant, Nanoparticles in radiation therapy: a summary of various approaches to enhance radiosensitization in cancer, Transl. Cancer Res. 2 (4) (2013) 330–342, https://doi.org/10.3978/j.issn.2218-676X.2013.08.06.
[70] S. Havaki, A. Kotsinas, E. Chronopoulos, D. Kletsas, A. Georgakilas, V.G. Gorgoulis, The role of oxidative DNA damage in radiation induced by stander effect, Cancer Lett. 356 (1) (2015) 43–51, https://doi.org/10.1016/j.canlet.2014.01.023.